bioRxiv preprint doi: https://doi.org/10.1101/756700; this version posted September 4, 2019. The copyright holder for this preprint (which was not certified by peer review) is the author/funder. All rights reserved. No reuse allowed without permission.

Temperature response of wheat affects final height and the timing of key developmental stages under field conditions

Lukas Kronenberg[a], Steven Yates[b], Martin P. Boer[c], Norbert Kirchgessner[a], Achim Walter[a], Andreas Hund[a]

[a] Crop Science, Institute of Agricultural Sciences , ETH Zürich, 8092 Zurich, Switzerland
[b] Molecular Plant Breeding, Institute of Agricultural Sciences , ETH Zürich, 8092 Zurich, Switzerland
[c] Biometris, Wageningen University & Research, 6708 PB Wageningen, The Netherlands

Abstract

In wheat, the timing and dynamics of stem elongation are tightly linked to temperature. It is yet unclear if and how these processes are genetically controlled. We aimed to identify quantitative trait loci (QTL) controlling temperature-response during stem elongation and to evaluate their relationship to phenology and height. Canopy height of the GABI wheat panel was measured between 2015 and 2017 in bi-weekly intervals in the field phenotyping platform (FIP) using a LIDAR. Temperature-response was modelled using a linear regression between stem elongation and the mean interval temperature.

The temperature-response was highly heritable (H^2 = 0.81) and positively related to a later start and end of stem elongation as well as an increased final height (FH). Genome-wide association mapping revealed three temperature-responsive and four temperature-irresponsive QTL. Furthermore, putative candidate genes for temperature-response QTL were frequently related to the flowering pathway in *A. thaliana* while temperature–irresponsive QTLs corresponded with growth and reduced height genes. These loci, together with the loci for start and end of stem elongation accounted for 49% of the variability in height.

This demonstrates how high throughput field phenotyping in combination with environmental covariates can contribute to a smarter selection of climate-resilient crops.

Key Words: field phenotyping, wheat, physiology, temperature-response, development, plant height

Introduction

Temperature is a major abiotic factor affecting plant growth and development. As a consequence of Global warming, wheat production could decrease by 6% per °C global temperature increase (Asseng *et al.*, 2015). While heat stress during critical stages can drastically reduce yield (Gibson and Paulsen, 1999; Farooq *et al.*, 2011), warm temperatures can decrease yield by accelerating development and thereby shortening critical periods for yield formation (Fischer, 1985; Slafer and Rawson, 1994). However little is known about how temperature affects development and growth, and how this is genetically controlled.

The critical phase for yield formation in wheat is stem elongation (SE); happening between the phenological stages of terminal spikelet initiation and anthesis (Slafer *et al.*, 2015). The

bioRxiv preprint doi: https://doi.org/10.1101/756700; this version posted September 4, 2019. The copyright holder for this preprint (which was not certified by peer review) is the author/funder. All rights reserved. No reuse allowed without permission.

start of SE coincides with the transition from vegetative to reproductive development, when the apex meristem differentiates from producing leaf primordia to producing spikelet primordia (Trevaskis *et al.*, 2007; Kamran *et al.*, 2014). During SE, florets are initiated at the spikelets until booting (Kirby, 1988; Slafer *et al.*, 2015). An increased duration of stem elongation increases the number of fertile florets due to longer spike growth and higher dry matter partitioning to the spike (González *et al.*, 2003). This in turn increases the number of grains per spike and therefore yield (Fischer, 1985). Modifying the timing of the critical phenological stages (transition to early reproductive phase and flowering) and SE duration has been proposed as way to increase wheat yield or at least mitigate adverse climate change effects on yield (Slafer *et al.*, 1996; Miralles and Slafer, 2007; Whitechurch *et al.*, 2007). The recent warming trend causes a faster advancement in phenology. For example over the past decade flowering time occurred earlier in Germany, which is attributable to both, increased temperature and selection for early flowering (Rezaei *et al.*, 2018).

Final height is also an important yield determinant. During the "green revolution" wheat yields increased by the introduction of reduced height genes (*Rht*). The resulting dwarf and semi dwarf varieties benefit from improved resource allocation from the stem to the spike and reduced lodging, allowing more intensive nitrogen application (Hedden, 2003). Gibberellin insensitive *Rht* genes (*Rht-A1*, *Rht-B1*, and *Rht-D1*) were shown limit cell wall extensibility which decreases growth rates (Keyes *et al.*, 1989) without affecting development (Youssefian *et al.*, 1992). Whilst the allele *Rht-B1c* (Wu *et al.*, 2011) and the GA sensitive *Rht12* dwarfing gene (Chen *et al.*, 2013) delay heading.

The main abiotic factors affecting the timing of floral initiation and flowering are temperature and photoperiod; with temperature affecting both vernalisation and general rate of development (Slafer *et al.*, 2015). These developmental transitions are controlled by major genes involved in the flowering pathway, namely; vernalisation (*VRN*), photoperiod (*PPD*) and earliness per se (*EPS*) genes (Slafer *et al.*, 2015). The *PPD* and *VRN* genes define photoperiod and vernalisation requirements which jointly enable the transition to generative development and define time to flowering. Whereas *EPS* genes fine tune the timing of floral transition and flowering, after vernalisation and photoperiod requirements are fulfilled (Zikhali and Griffiths, 2015). While vernalisation and photoperiod response are well known, the role of temperature *per se* remains less clear. Temperature affects all developmental phases and warmer ambient temperatures generally accelerate growth and development in crops (Slafer and Rawson, 1994, 1995*a*,*c*; Atkinson and Porter, 1996; Fischer, 2011; Slafer *et al.*, 2015). But it is unclear, if temperature-response governs growth rate and development independently. If so, the question remains whether there is enough genetic variability in temperature-response to be used in a breeding context (Parent and Tardieu, 2012).

Genotypic variation for growth response to temperature was reported for wheat leaf elongation rate (Nagelmüller *et al.*, 2016), as well as for canopy cover growth (Grieder *et al.*, 2015). Kiss *et al.* (2017) reported significant genotype by temperature interactions in the timing of stem elongation as well as temperature dependent differences in the expression of *VRN* and *PPD* genes under controlled conditions. Under field conditions, the response of stem elongation to temperature has not yet been investigated in high temporal resolution.

bioRxiv preprint doi: https://doi.org/10.1101/756700; this version posted September 4, 2019. The copyright holder for this preprint (which was not certified by peer review) is the author/funder. All rights reserved. No reuse allowed without permission.

In recent years, new high throughput phenotyping technologies have enabled monitoring plant height with high accuracy and frequency in the field (Bendig *et al.*, 2013; Friedli *et al.*, 2016; Holman *et al.*, 2016; Aasen and Bareth, 2018; Hund *et al.*, 2019). We have previously demonstrated that the ETH field phenotyping platform (FIP, Kirchgessner *et al.*, 2016) can be used to accurately track the development of canopy height in a large set of wheat genotypes using terrestrial laser scanning (Kronenberg *et al.*, 2017). Considerable genotypic variation was detected for the start and end of SE which correlated positively with final canopy height (Kronenberg *et al.*, 2017).

While many temperature-independent factors affecting plant height are known, the influences of temperature-dependent elongation and timing of the elongation phase is less clear. To address this, we aimed to dissect final height into the following components: i) temperature-independent elongation, ii) temperature-dependent elongation and iii) the duration of the elongation phase determining by the start and end of the process. To achieve this we present a method to assess and measure these three processes under field conditions by means of high-frequency, high-throughput phenotyping of canopy height development. The resulting data were combined with genetic markers to identify quantitative trait loci controlling the aforementioned processes.

Material and Methods

Experimental setup, phenotyping procedures and extracted traits

Field experiments were conducted in the field phenotyping platform FIP at the ETH research station in Lindau-Eschikon, Switzerland (47.449°N, 8.682°E, 520 m a.s.l.; soil type: eutric cambisol). We used a set of approximately 330 winter wheat genotypes (335 – 352 depending on the experiment) comprising current European elite cultivars (GABI Wheat; Kollers *et al.*, 2013), supplemented with thirty Swiss varieties. These were monitored over three growing seasons in 2015, 2016 and 2017. Details about the experimental setup for the growing seasons 2015 and 2016 are described in Kronenberg *et al.* (2017). Briefly, the field experiments were conducted in an augmented design with two replications per genotype using micro plots with a size of 1.4 by 1.1 m. In the growing season 2017, the experiment was repeated again, with minor changes in genotypic composition. This resulted in 328 genotypes present across all three experiments.

Canopy height was measured twice weekly from the beginning of shooting (BBCH 31) until final height using a light detection and ranging (LIDAR) scanner (FARO R Focus3D S 120; Faro Technologies Inc., Lake Mary USA) mounted on the FIP (Kirchgessner *et al.*, 2016). Canopy height data was extracted from the LIDAR data as described in Kronenberg et al. (2017). Spatial heterogeneity at each measuring date was corrected by applying two-dimensional P-splines to the raw canopy height data within each year using the R-package SpATS (Rodríguez-Álvarez *et al.*, 2018). The start, end, and duration of stem elongation with final canopy height (FH) were extracted from the height data as described by Kronenberg *et al.* (2017): Normalized canopy height was calculated as percent of final height at each day of measurement for every plot and then linearly interpolated between measurement points. Growing degree-days until 15% final height (GDD_{15}) and 95% final height (GDD_{95}) were used as proxy traits for start and end of stem elongation, respectively. SE duration was recorded in thermal time (GDD_{SE}) as

bioRxiv preprint doi: https://doi.org/10.1101/756700; this version posted September 4, 2019. The copyright holder for this preprint (which was not certified by peer review) is the author/funder. All rights reserved. No reuse allowed without permission.

well as in calendar days ($time_{SE}$), as the difference between GDD_{95} and GDD_{15} (Kronenberg *et al.*, 2017).

In order to investigate short-term growth response to temperature, average daily stem elongation rates (SER) were calculated for each plot as the difference (Δ) in canopy height (CH) between consecutive timepoints (t):

$$SER = \frac{\Delta CH}{\Delta t} \quad \text{eq. 1}$$

Extracting growth response to temperature

Temperature response was modelled by regressing average daily stem elongation rates (SER) against average temperature of the respective interval for each plot within the respective year following

$$SER = (a \times T) + b_{T_{crit}} + \varepsilon \quad \text{eq. 2}$$

where *T* is the ambient temperature, *a* is the coefficient of the linear regression (i.e. growth response to ambient temperature; $slp_{SER\sim T}$) and *ε* denotes the residual error. b_{Tcrit} is the model intercept, estimated at the temperature, at which the correlation between intercept and slope is zero ($int_{SER\sim T}$). *Tcrit* was determined empirically for each year by sequentially estimating the intercept between 1°C and 22°C Fig. 1A). Per definition, the intercept would be estimated at T = 0 °C, i.e. far outside the range of observed temperatures. In the observed data, an intercept at T = 0°C correlated strongly negative with the slope (Fig. 1A) and, thus, did not add much additional information concerning the performance of the evaluated genotypes. Grieder et al. (2015) performed a similar analysis for the canopy cover development during winter and found a similar, strongly negative correlation between temperature-response (slope) and growth at 0°C (intercept). Likewise an intercept at 20°C at the upper range of the observed data was correlated strongly positive with the slope. Hence, T_{crit} is the turning point from negative to positive correlation as the position of the intercept increases, which is the point where intercept and slope are independent. Therefore, two genotypes can show the same growth at T_{crit} but differ markedly in temperature-response (Fig. 1B), have the same temperature-response but differ in growth at T_{crit} (Fig. 1C), or differ for both, intercept and slope (Fig. 1D). Following this, $int_{SER\sim T}$ would be interpreted as intrinsic, temperature-independent growth, hereinafter referred to as “vigour”.

Statistical Analysis

All statistical analysis were performed in the R environment (R Core Team, 2018). Best linear unbiased estimations (BLUEs), predictors (BLUPs) and broad sense heritabilities (H^2) were determined for all traits using the R-package *asreml* (Butler, 2009). In a first step, BLUEs were calculated within each year using:

$$Y = \mu + g + \varepsilon \quad \text{eq. 3}$$

Where *Y* is the respective trait (FH, GDD_{15}, GDD_{95}, GDD_{SE}, $int_{SER\sim T}$ or $slp_{SER\sim T}$), μ is the overall mean, *g* the fixed genotype effect and ε is the residual error.

In a second step, 3-year BLUPs were calculated using

bioRxiv preprint doi: https://doi.org/10.1101/756700; this version posted September 4, 2019. The copyright holder for this preprint (which was not certified by peer review) is the author/funder. All rights reserved. No reuse allowed without permission.

$$Y = \mu + g + y + \varepsilon \quad \text{eq. 4}$$

where Y are the single-year BLUEs for the respective traits derived from eq. 3, μ is the overall mean, g is the genotype effect, y is the year effect and ε is the residual error. Broad sense heritabilities were calculated following Falconer and Mackay (1996) as

$$H^2 = \frac{\sigma_G^2}{\sigma_G^2 + \frac{\sigma_\varepsilon^2}{3}} \quad \text{eq. 5}$$

where σ_G^2 and σ_ε^2 are genotypic and residual variance, respectively, from eq. 4.

The 3-year BLUPs of GDD_{15}, GDD_{95}, GDD_{SE}, FH, $int_{SER\sim T}$, and $slp_{SER\sim T}$ were used for correlations and genome wide association study (GWAS).

Association study

The genetic basis of temperature-response was investigated by GWAS. GWAS was performed on the different traits to compare the phenotypic correlations with the underlying genetic architecture of the traits. As a positive control final height data made in Germany and France by Zanke *et al.* (2014*b*) was also compared and analysed.

Genotyping data was made previously by the GABI wheat consortium represented by the Leibniz Institute of Plant Genetics and Crop Plant Research (IPK; Zanke *et al.*, 2014*a*) using the 90K illumina SNP-chip (Cavanagh *et al.*, 2013; Wang *et al.*, 2014). Monomorphic SNPs were discarded. The remaining markers were mapped to the IWGSC reference genome (Consortium (IWGSC) *et al.*, 2018) by BLASTN search using an E-value threshold < $1e^{-30}$. The genome position with the lowest E-value was assigned as the respective marker location. Markers that could not be unequivocally positioned were dropped. After filtering SNPs with a minor allele frequency and missing genotype rate < 0.05, a total of 13,450 SNP markers and 315 genotypes remained in the set. The reference genome position of *RHT*, *PPD*, *VRN* and putative *EPS* genes was determined with BLASTN search as described above using published GenBank sequences (Table S1).

To mitigate against multiple testing, relatedness and population structure; three different methods were used to calculate marker trait associations (MTA) between phenotypic BLUPs and SNP markers:

i) We used a mixed linear model (MLM) including principal components among marker alleles as fixed effects and kinship as random effect to account for population structure (Zhang *et al.*, 2010). This approach was chosen to stringently prevent type I errors. The MLM GWAS was performed using the R Package GAPIT (v.2, Tang *et al.*, 2016). Kinship was estimated according to VanRaden (2008).

ii) In a generalised linear model (GLM) framework implemented in PLINK (Purcell *et al.*, 2007), association analysis was performed using SNP haplotype blocks consisting of adjacent SNP triplets. Using haplotype blocks takes the surrounding region of a given SNP into account, thus increasing the power to detect rare variants (Purcell *et al.*, 2007)

iii) Finally, the FarmCPU method (Liu *et al.*, 2016) was used, which is also implemented in GAPIT. FarmCPU tests individual markers with multiple associated markers as

bioRxiv preprint doi: https://doi.org/10.1101/756700; this version posted September 4, 2019. The copyright holder for this preprint (which was not certified by peer review) is the author/funder. All rights reserved. No reuse allowed without permission.

covariates in a fixed effect model. Associated markers are iteratively used in a random effect model to estimate kinship. Confounding between testing markers and kinship is thus removed while controlling type I error, leading to increased power (Liu *et al.*, 2016).

For all methods, a Bonferroni correction was applied to the pointwise significance threshold of $\alpha = 0.05$, to avoid false-positives. Hence, only markers above $-\log_{10}(P\text{-value}) >= 5.43$ considered significant.

Linkage disequilibrium (LD) among markers was estimated using the squared correlation coefficient (r^2) calculated with the R package SNPrelate (Zheng *et al.*, 2012). A threshold of $r^2 = 0.2$ (Gaut and Long, 2003) was applied to calculate the chromosome specific distance threshold of LD decay. Putative candidate genes were identified by searching the IWGSC annotation of the reference genome (Consortium (IWGSC) *et al.*, 2018) for genes associated with growth and development within the LD distance threshold around the respective MTA.

Results

Phenotypic results

We measured the canopy height of 710 – 756 plots per year, containing 335 – 352 wheat genotypes, for three consecutive years. In each season measurements were made between 17 and 22 times during stem elongation. Thus resulting in an average of 122 canopy height measurement points per genotype. From these data we extracted growth rates and the timing of critical stages. Plot based growth rates within single years indicate a clear relation between growth and temperature for the period of stem elongation, as depicted in Fig. 2. Towards the end of the measurement period in June, there was a larger deviation, which was also reflected in the quality of plot based linear model fits of SER versus temperature (*see* eq. 2), summarized in Fig. S1. For the 2015 and especially the 2016 experiment, R^2 values were low and except for the 2017 experiment, the parameter estimates were not statistically significant (Fig. S1A). Inspection of the best and worst model fits however shows, that failure of fitting the model for single plots was levelled out by the replications within genotypes (Fig. S1B), therefore allowing for confident estimates of genotypic means of the model parameters (see below). Analysis of variance revealed significant ($P < 0.001$) genotypic effects for both $slp_{SER\sim T}$ and $int_{SER\sim T}$ within single years as well as across three years. Both traits showed high heritabilities across years ($H^2 = 0.81$ for $slp_{SER\sim T}$ and $H^2 = 0.77$ for $int_{SER\sim T}$) and very high heritabilities within single years (Table 1). Using the BLUPs of $slp_{SER\sim T}$, $int_{SER\sim T}$ and temperature sum for stem elongation (GDD_{SE}), final height could be predicted with high accuracy across different years ($0.82 <= R^2 <= 0.85$) by training a linear model on the BLUPs of one year and predicting it on the BLUPs of another independent year. Training the model on the 3-year BLUPs resulted in a prediction accuracy of single years between $R^2 = 0.93$ and $R^2 = 0.95$ (Fig. 3). High heritabilities within years ($0.75 <= H^2 <= 0.99$) as well as across three years ($0.54 <= H^2 <= 0.98$; Table 1), were also found for other traits; final height, start of SE, end of SE and SE duration.

Phenology, temperature-response and final height were positively correlated

bioRxiv preprint doi: https://doi.org/10.1101/756700; this version posted September 4, 2019. The copyright holder for this preprint (which was not certified by peer review) is the author/funder. All rights reserved. No reuse allowed without permission.

To evaluate the relationships between the traits measured, Pearson correlation coefficients were calculated for each trait pair. If not indicated otherwise, the reported correlations were highly significant ($P < 0.001$)

Positive correlations were found among GDD_{15}, GDD_{95} and FH ($0.36 <= r <= 0.64$, Fig. 4), indicating that taller varieties were generally later. Temperature response ($slp_{SER\sim T}$) and vigour ($int_{SER\sim T}$) also showed a strong, positive relationship with final height ($r = 0.85$ and $r = 0.65$, respectively). However, only temperature-response correlated with GDD_{15} and GDD_{95} ($r = 0.63$ and $r = 59$, respectively), whereas vigour did not ($r < 0.26$, Fig. S2).

As expected, stem elongation duration in thermal time (GDD_{SE}) was negatively correlated with GDD_{15} ($r = -0.44$) and positively correlated with GDD_{95} ($r = 0.4$). But, GDD_{SE} did not correlate with final height ($r = -0.01$, $P = 0.878$) or temperature-response ($r = 0.006$, $P = 0.289$). Although GDD_{SE} negatively correlated with vigour ($r = -0.32$). In contrast, SE duration in calendar days ($time_{SE}$) was negatively correlated with temperature-response ($r = -0.35$) and GDD_{15} ($r = -0.82$), indicating a longer SE phase for earlier genotypes. Other weak correlations ($r < 0.3$), that are not discussed, are shown in Fig. S2.

Linkage disequilibrium and population structure

Prior to MTA analysis we evaluated population structure and LD. Principal component analysis of the marker genotypes revealed no distinct substructure in the investigated population. The biplot of the first two principal components showed no apparent clusters, with the first component explaining 8% and the second component explaining 3.3% of the variation in the population (Fig. S5). This is consistent with prior work using the same population (Kollers *et al.*, 2013; Yates *et al.*, 2018). On average across all chromosomes, LD decayed below an r^2 of 0.2 at a distance of 9 MB. There was however considerable variation in this threshold among the single chromosomes (Table S2).

Association study

Genome-wide association results differed markedly depending on the applied model. Using a MLM with kinship matrix and PCA as covariates resulted in no significant MTA for any trait (Fig. S3). In contrast, the GLM using the haplotype method yielded 2949 significant MTA for $\alpha < 0.05$ and 1846 MTA for $\alpha < 0.001$ respectively. However, investigation of the respective QQ-plots showed large *P*-value inflation in the haplotype method whereas the *P*-values were slightly deflated when using the MLM approach (Fig. S3, Fig. S4). In contrast, with FamCPU the QQ-plots (Fig. 5) showed no *P*-value inflation, except for some markers. This pattern is expected, if population structure is appropriately controlled. Therefore, FarmCPU was chosen to be the most appropriate method for the given data, despite identifying less significant MTA.

As a positive control we compared our final height data and associated markers with data made by Zanke *et al.* (2014*b*). Final canopy height correlated strongly between the two studies ($r = 0.95$), which is in accordance with the high heritability of the trait. In this study, we found 11 significant MTA for final height (Table 2, Fig. 5). Zanke *et al.* (2014*b*) reported 280 significant MTA for final height across several environments. Of these, only marker RAC875_rep_c105718_585 on chromosome 4D overlapped with the MTA found in this study. However, by considering flanking markers, we found that of the remaining ten significant MTA

bioRxiv preprint doi: https://doi.org/10.1101/756700; this version posted September 4, 2019. The copyright holder for this preprint (which was not certified by peer review) is the author/funder. All rights reserved. No reuse allowed without permission.

for final height, six were in LD with MTA found by Zanke *et al.* (2014*b*; Table S3). The significant MTA found for FH in this study are near known genes controlling FH. For example, Tdurum_contig64772_417, is 4 MB upstream of *Rht*-B1 and RAC875_rep_c105718_585, is 7 MB downstream of *Rht*-D1 on their respective group 4 chromosomes.

Temperature-response loci are independent of vigour loci

For $slp_{SER\sim T}$ we detected one significant (LOD = 5.77) MTA on chromosome 1B (wsnp_Ex_c1597_3045682) and two almost significant (LOD = 5.39 / LOD = 5.02) MTA on chromosomes 4B (CAP7_c10839_300) and 5D (IAAV7104), respectively (Fig. 5). All associated markers for $slp_{SER\sim T}$ yielded small but significant allelic effects ranging from -0.049 mm $°C^{-1}d^{-1}$ to -0.041 mm $°C^{-1}d^{-1}$ (Table 2). The GWAS for $int_{SER\sim T}$ yielded four significant MTA on chromosomes 2B, 4B, 4D and 5D respectively (Table 2, Fig. 5). Start and end of SE yielded four MTA each (Table 2, Fig. 5).

Comparing the GWAS results for temperature-response, vigour, final height, GDD_{15} and GDD_{95} revealed no common quantitative trait loci (QTL) between $slp_{SER\sim T}$ and any other trait. Only one marker (Excalibur_c74858_243) was significantly associated with both GDD_{15} as well as GDD_{95}. The lack of overlap, of MTA, between temperature-response, vigour and timing of critical stages indicate they are genetically independent. However, there is a genetic connection between vigour and FH on the one hand and between the start and end of stem elongation on the other.

To identify potential causative genes underlying the QTL, we searched the reference genome annotation around the respective QTL intervals. For temperature-response we found an increased presence of genes or gene homologues involved in the flowering pathway, i.e. EARLY FLOWERING 3, FRIGIDA and CONSTANS (Table 3). Around the QTL associated with vigour the annotation showed genes associated with growth (i.e. GRAS, CLAVATA, BSU1, Argonaute) as well as developmental progress (i.e. Tesmin/TSO1-like CXC domain, BEL1, AGAMOUS (Table 4). Importantly, we found *GAI-like protein 1* 6MB upstream of marker Kukri_rep_c68594_530, which we identified as *RHT-D1* by blasting the *RHT*-D1 sequence (GeneBank ID AJ242531.1) against the annotated reference genome.

Vigour, temperature-response and the timing of SE affect final height

The phenotypic correlations show a strong connection between temperature-response, vigour and FH as well as weaker connections between GDD_{15}, GDD_{95} and FH. In order to examine this interdependency on a genetic level, we used a linear model to predict FH with the SNP alleles of the QTL for $slp_{SER\sim T}$, $int_{SER\sim T}$, GDD_{15} and GDD_{95} as predictors. The model was able to predict FH with an accuracy $R^2 = 0.49$, with significant contributions by QTL of all three traits (Fig. 6, Table 5).

Discussion

In this study we present a method to measure temperature response during stem elongation of wheat using high throughput phenotyping of canopy height in the field. The results show a highly heritable genotype-specific ambient temperature response of wheat which affects both growth and timing of the developmental key stages. We modelled temperature-response in a

bioRxiv preprint doi: https://doi.org/10.1101/756700; this version posted September 4, 2019. The copyright holder for this preprint (which was not certified by peer review) is the author/funder. All rights reserved. No reuse allowed without permission.

simple linear framework with the intercept estimated at the temperature of zero correlation to the slope. This allowed for the decomposition of growth dynamics into a genotype-specific vigour component and temperature-response component. Thereby we could assess interdependence between vigour and temperature-response to plant height and the timing of developmental key stages.

Linear models were used before to describe wheat growth response to temperature for leaf elongation (Nagelmüller *et al.*, 2016), canopy cover (Grieder *et al.*, 2015) as well as stem elongation rate (Slafer and Rawson, 1995*a*). Others proposed the use of a more complex, Arrhenius type of function to account for decreasing growth rates at supra optimal temperatures (Parent and Tardieu, 2012). Wheat has its temperature-optimum at around 27°C (Parent and Tardieu, 2012). As temperatures in the measured growth intervals during stem elongation did not exceed 25°C and given the temporal resolution of the data, a simple linear model is justified (Parent *et al.*, 2018).

The results of the correlation analysis show a clear connection between FH and temperature-response ($slp_{SER\sim T}$) as well as between FH and vigour ($int_{SER\sim T}$). This is consistent with part i) and ii) of our hypothesis: Final height can be described as a function of temperature-independent growth processes and as a function of temperature-response during SE. Importantly, among all components, the temperature-response was a major driver of final height and also had a strong influence on the timing. Temperature-response delayed the beginning of stem elongation leading to a later start and end of the whole phase. This finding might appear counter intuitive: given the assumption that plants develop faster under higher ambient temperatures a more responsive genotype should develop faster compared to a less responsive one. Slafer and Rawson (1995*b*) reported an accelerated development towards floral transition with increasing temperatures up to 19°C whereas higher temperatures slowed development. In that respect, a more responsive genotype would experience a stronger delay of floral transition under warm temperatures.

In terms of their correlation to FH, the effects of the timing of start and end of stem elongation (part iii) of the initial hypothesis) are less distinct. Final height was more a function of faster growth than duration of growth, especially since genotypes with a strong temperature-response have a shorter duration of SE. However, the timing of start and end of stem elongation was linked with temperature-response. Based on this result and the according correlations, it would appear that temperature-response influences FH directly as well as indirectly by mediating start and end of stem elongation.

The question, whether these trait correlations are due to pleiotropic effects will substantially impact the breeding strategy (Chen and Lübberstedt, 2010). If these effects are pleotropic, they have a huge impact on breeding as they indicate that temperature-response, timing and height are to a large degree determined by the same set of genes. Alternative explanations are linkage and population structure. As the examined traits are major drivers of adaptation to the different regions of Europe we anticipate a very strong selection for both, temperature response as well as timing of critical stages. The GABI wheat panel is made of wheat varieties from different regions of Europe. Even if there is no apparent population structure at neutral markers, there may be a strong population structure at selected loci with strong effect on local

bioRxiv preprint doi: https://doi.org/10.1101/756700; this version posted September 4, 2019. The copyright holder for this preprint (which was not certified by peer review) is the author/funder. All rights reserved. No reuse allowed without permission.

adaptation. However, pleiotropy between height and flowering time is known for maize and rice, supporting the hypothesis of pleiotropy here. The *DWARF8* gene of maize encoding a DELLA protein is associated with height and flowering time (Lawit *et al.*, 2010) and strongly associated with climate adaptation (Camus-Kulandaivelu *et al.*, 2006, page). The rice *GHD7* locus has a strong effect on number of days to heading, number of grains per panicle, plant height and stem growth (Xue *et al.*, 2008). To further examine the relationship among the different traits we consider the following GWAS analysis using stringent correction of population structure.

The GWAS results indicate an independent genetic control of final height, temperature response and the timing of critical stages. Whereas vigour and FH as well as start and end of SE appear to be partly linked. Yet, final height could be predicted with surprising accuracy using the QTL for temperature response, vigour, start and end of SE which reflects the correlations found in the phenotypic data.

Previous studies investigating the control of developmental key stages in wheat with respect to temperature generally adopted the concept, that after fulfilment of photoperiod and vernalisation, *EPS* genes act as fine tuning factors independent of environmental stimuli (Kamran *et al.*, 2014; Zikhali and Griffiths, 2015). Temperature, apart from vernalisation is thought to generally quicken growth and development independent of the cultivar (Slafer and Rawson, 1995*b*; Porter and Gawith, 1999; Slafer *et al.*, 2015). A genotype-specific temperature effect on the duration of different phases was not considered (Takahashi &Yasuda 1971, Slafer & Rawson 1995c). It was however reported, that photoperiod effects vary depending on temperature (Slafer and Rawson, 1995*c*). Under long days, Hemming *et al.* (2012) reported faster development and fewer fertile florets under high compared to low temperatures. Temperature-dependent effects were also found for different *EPS* QTL (Slafer and Rawson, 1995*c*; Gororo *et al.*, 2001). It has previously been suggested, that *EPS* effects could be associated with interaction effects between genotype and temperature fluctuations (Slafer and Rawson, 1995*c*; van Beem *et al.*, 2005).

The mechanisms of ambient temperature sensing and its effects on growth and development are not yet well understood (Sanchez-Bermejo and Balasubramanian, 2016). However, important findings regarding ambient temperature effects on flowering time as well as on hypocotyl elongation have come from the model species *Arabidopsis thaliana* (Wigge, 2013). With respect to these two traits, Sanchez-Bermejo and Balasubramanian (2016) reported distinct genotypic differences in temperature-sensitivity. According to their results, the flowering pathway genes FRIGIDA (*FRI*), FLOWERING LOCUS C (*FLC*) and FLOWERING LOCUS T (*FT*) are major candidate genes for ambient temperature mediated differences in flowering time (Sanchez-Bermejo and Balasubramanian, 2016). In the present study, we found *FRI* homologues near two of the three QTL for temperature-response. *FRI* and *FLC* acts as main vernalisation genes in *A. thaliana* (Johanson *et al.*, 2000; Amasino and Michaels, 2010). In wheat, these genes are not yet well described. However, *FLC* orthologues were found to act as flowering repressors regulated by vernalisation in monocots (Sharma *et al.*, 2017).

Another promising candidate gene for temperature response found near the QTL on chromosome 1B is EARLY FLOWERING 3 (*ELF3*). In *A. thaliana*, *ELF3* was found to be a core

bioRxiv preprint doi: https://doi.org/10.1101/756700; this version posted September 4, 2019. The copyright holder for this preprint (which was not certified by peer review) is the author/funder. All rights reserved. No reuse allowed without permission.

part of circadian clock involved in ambient temperature response (Thines and Harmon, 2010). In Barley, *ELF3* was shown to be involved in the control of temperature dependent expression of flowering time genes (Ejaz and von Korff, 2017). A mutant *ELF3* accelerated floral development under high ambient temperatures while maintaining the number of seeds (Ejaz and von Korff, 2017). Furthermore, *ELF3* has been reported as a candidate gene for *EPS1* in *Triticum monococcum* (Alvarez *et al.*, 2016).

One important aspect we could not address in the current study is the interaction of genotype specific temperature response with vernalisation and photoperiod (Slafer and Rawson, 1995*c*; Gol *et al.*, 2017; Kiss *et al.*, 2017). It also remains unclear if and to which extent temperature response varies across different developmental phases and how temperature-response relates to other environmental stimuli such as vapour pressure deficit or radiation. Nevertheless, the results of this study present valuable information towards a better understanding of temperature response in wheat and may be of great importance for breeding. Temperature-response could provide a breeding avenue for local adaptation as well as the control of plant height.

With the recent advancements in UAV-based phenotyping techniques, the growth of canopy cover and canopy height can be measured using image segmentation and structure from motion approaches (Bareth *et al.*, 2016; Aasen and Bareth, 2018; Roth *et al.*, 2018). Thus, temperature-response can be investigated during the vegetative canopy cover development (Grieder *et al.*, 2015) and during the generative height development as demonstrated here. It can also be assessed in indoor platforms (e.g. Parent and Tardieu, 2012) and the field using leaf length tracker (Nagelmüller *et al.*, 2016) measuring short-term responses of leaf growth to diurnal changes in temperature. Combining this information may greatly improve our understanding about the genetic variation in growth response to temperature.

Conclusion

Modern phenotyping platforms hold great promise to map the genetic factors driving the response of developmental processes to environmental stimuli. To the best of our knowledge, this is the first experiment dissecting the stem elongation process into its underlying components: temperature-dependent elongation, temperature-independent vigour and elongation duration. The independent loci detected for these traits, suggest that it is possible to select them independently. The detected loci may be used to fine tune height and the beginning and end of stem elongation as they explain a substantial part of the overall genotypic variation. With increases in automation, growth processes may be monitored in the field on a daily basis or even multiple times per day. This will increasing the precision in assessing genotype responses to the fluctuation in meteorological conditions and quantifying the relationship of these responses to yield. Remote sensing by means of unmanned aerial vehicles in combination with photogrammetric algorithms will allow to measure these traits in breeding nurseries. We believe that this is paving the road for a more informed selection to climate adaptation within individual growing seasons.

Supplementary Data

Fig. S1: Summary of plot based linear model fits of stem elongation rate vs. temperature.

bioRxiv preprint doi: https://doi.org/10.1101/756700; this version posted September 4, 2019. The copyright holder for this preprint (which was not certified by peer review) is the author/funder. All rights reserved. No reuse allowed without permission.

Fig. S2: Pearson correlation coefficients among 3-year BLUPS of all investigated traits.

Fig. S3: Manhattan plots and quantile-quantile plots depicting the GWAS results using the MLM approach.

Fig. S4: Manhattan plots and quantile-quantile plots depicting the GWAS results using the GLM approach.

Fig. S5: Principal component analysis among marker genotypes.

Table S1: Genes of interest related to floral transition and flowering.

Table S2: Chromosome wise distance thresholds for LD-decay < $r^2 = 0.2$.

Table S3: Corresponding marker-trait associations for final canopy height with respect to Zanke et al. 2016.

Table S4: 3-year BLUPs of the investigated traits FH, GDD_{15}, GDD_{95}, GDD_{SE}, $time_{SE}$, $slp_{SER\sim T}$, $int_{SER\sim T}$.

Acknowledgements

We sincerely thank Hansueli Zellweger for managing and nursing our field experiments. We further thank the members of the ETH crop science and the ETH molecular plant breeding groups, especially Michelle Nay and Beat Keller, for many fruitful discussions. We also thank Martina Binder for doing the correlation analysis between the final height data of this study and the data made by Zanke *et al.* (2014*b*) in the framework of her MSc-Thesis. We would like to thank Marion Röder (IPK Gatersleben) for supply of the GABI wheat panel including genetic information. Finally, we thank the anonymous reviewers for their helpful comments and suggestions. This work was supported by the Swiss National Foundation (SNF) in the framework of the project PhenoCOOL (project no. 169542).

Author contribution

LK conducted the laser scans, did all statistical analyses and drafted the manuscript; SY assisted with the GWAS and candidate gene evaluation; MB assisted with the spatial correction; NK developed the analysis pipeline for the laser scans; AW drafted the grant application and supervised the overall concept; AH made the experimental design, developed the phenotyping models and assisted with the statistical analysis. All authors contributed to the drafting of the manuscript.

References

Aasen H, Bareth G. 2018. Spectral and 3D Nonspectral Approaches to Crop Trait Estimation Using Ground and UAV Sensing. In: Thenkabail PS, Lyon JG, Huete A, eds. Hyperspectral Remote Sensing Of Vegetation. Biophysical and Biochemical Characterization and Plant Species Studies. 103–131.

Alvarez MA, Tranquilli G, Lewis S, Kippes N, Dubcovsky J. 2016. Genetic and physical mapping of the earliness per se locus Eps-Am1 in Triticum monococcum identifies EARLY FLOWERING 3 (ELF3) as a candidate gene. Functional & Integrative Genomics **16**, 365–382.

bioRxiv preprint doi: https://doi.org/10.1101/756700; this version posted September 4, 2019. The copyright holder for this preprint (which was not certified by peer review) is the author/funder. All rights reserved. No reuse allowed without permission.

Amasino RM, Michaels SD. 2010. The Timing of Flowering. Plant Physiology **154**, 516–520.

Asseng S, Ewert F, Martre P, *et al.* 2015. Rising temperatures reduce global wheat production. Nature Climate Change **5**, 143–147.

Atkinson D, Porter JR. 1996. Temperature, plant development and crop yields. Trends in Plant Science **1**, 119–124.

Bareth G, Bendig J, Tilly N, Hoffmeister D, Aasen H, Bolten A. 2016. A Comparison of UAV- and TLS-derived Plant Height for Crop Monitoring: Using Polygon Grids for the Analysis of Crop Surface Models (CSMs). Photogrammetrie - Fernerkundung - Geoinformation **2016**, 85–94.

van Beem J, Mohler V, Lukman R, van Ginkel M, William M, Crossa J, Worland AJ. 2005. Analysis of Genetic Factors Influencing the Developmental Rate of Globally Important CIMMYT Wheat Cultivars. Crop Science **45**, 2113–2119.

Bendig J, Bolten A, Bareth G. 2013. UAV-based Imaging for Multi-Temporal, very high Resolution Crop Surface Models to monitor Crop Growth Variability. PFG Photogrammetrie, Fernerkundung, Geoinformation, 551–562.

Butler D. 2009. *asreml: asreml() fits the linear mixed model*.

Camus-Kulandaivelu L, Veyrieras J-B, Madur D, Combes V, Fourmann M, Barraud S, Dubreuil P, Gouesnard B, Manicacci D, Charcosset A. 2006. Maize Adaptation to Temperate Climate: Relationship Between Population Structure and Polymorphism in the Dwarf8 Gene. Genetics **172**, 2449–2463.

Cavanagh CR, Chao S, Wang S, *et al.* 2013. Genome-wide comparative diversity uncovers multiple targets of selection for improvement in hexaploid wheat landraces and cultivars. Proceedings of the National Academy of Sciences **110**, 8057–8062.

Chen Y, Lübberstedt T. 2010. Molecular basis of trait correlations. Trends in Plant Science **15**, 454–461.

Chen L, Phillips AL, Condon AG, Parry MAJ, Hu Y-G. 2013. GA-Responsive Dwarfing Gene Rht12 Affects the Developmental and Agronomic Traits in Common Bread Wheat. PLoS ONE **8**.

Consortium (IWGSC) TIWGS, Investigators IR principal, Appels R, *et al.* 2018. Shifting the limits in wheat research and breeding using a fully annotated reference genome. Science **361**, eaar7191.

Ejaz M, von Korff M. 2017. The Genetic Control of Reproductive Development under High Ambient Temperature. Plant Physiology **173**, 294–306.

Falconer DS, Mackay TF. 1996. *Introduction to Quantitative Genetics*. Essex, England: Benjamin Cummings.

Farooq M, Bramley H, Palta JA, Siddique KHM. 2011. Heat Stress in Wheat during Reproductive and Grain-Filling Phases. Critical Reviews in Plant Sciences **30**, 491–507.

bioRxiv preprint doi: https://doi.org/10.1101/756700; this version posted September 4, 2019. The copyright holder for this preprint (which was not certified by peer review) is the author/funder. All rights reserved. No reuse allowed without permission.

Fischer RA. 1985. Number of kernels in wheat crops and the influence of solar radiation and temperature. The Journal of Agricultural Science **105**, 447–461.

Fischer RA. 2011. Wheat physiology: a review of recent developments. Crop and Pasture Science **62**, 95–114.

Friedli M, Kirchgessner N, Grieder C, Liebisch F, Mannale M, Walter A. 2016. Terrestrial 3D laser scanning to track the increase in canopy height of both monocot and dicot crop species under field conditions. Plant Methods **12**, 9.

Gaut BS, Long AD. 2003. The Lowdown on Linkage Disequilibrium. The Plant Cell **15**, 1502–1506.

Gibson LR, Paulsen GM. 1999. Yield Components of Wheat Grown under High Temperature Stress during Reproductive Growth. Crop Science **39**, 1841–1846.

Gol L, Tomé F, von Korff M. 2017. Floral transitions in wheat and barley: interactions between photoperiod, abiotic stresses, and nutrient status. Journal of Experimental Botany **68**, 1399–1410.

González FG, Slafer GA, Miralles DJ. 2003. Floret development and spike growth as affected by photoperiod during stem elongation in wheat. Field Crops Research **81**, 29–38.

Gororo NN, Flood RG, Eastwood RF, Eagles HA. 2001. Photoperiod and Vernalization Responses in Triticum turgidum × T. tauschii Synthetic Hexaploid Wheats. Annals of Botany **88**, 947–952.

Grieder C, Hund A, Walter A. 2015. Image based phenotyping during winter: a powerful tool to assess wheat genetic variation in growth response to temperature. Functional Plant Biology **42**, 387–396.

Hedden P. 2003. The genes of the Green Revolution. Trends in Genetics **19**, 5–9.

Hemming MN, Walford SA, Fieg S, Dennis ES, Trevaskis B. 2012. Identification of High-Temperature-Responsive Genes in Cereals. Plant Physiology **158**, 1439–1450.

Holman F, Riche A, Michalski A, Castle M, Wooster M, Hawkesford M. 2016. High Throughput Field Phenotyping of Wheat Plant Height and Growth Rate in Field Plot Trials Using UAV Based Remote Sensing. Remote Sensing **8**, 1031.

Hund A, Kronenberg L, Anderegg J, Yu K, Walter A. 2019. Non-invasive field phenotyping of cereal development. In: Ordon F, Friedt W, eds. Advances in breeding techniques for cereal crops. Cambridge UK: Buleigh Dodds Science Publishing.

Johanson U, West J, Lister C, Michaels S, Amasino R, Dean C. 2000. Molecular Analysis of FRIGIDA, a Major Determinant of Natural Variation in Arabidopsis Flowering Time. Science **290**, 344–347.

Kamran A, Iqbal M, Spaner D. 2014. Flowering time in wheat (Triticum aestivum L.): a key factor for global adaptability. Euphytica **197**, 1–26.

bioRxiv preprint doi: https://doi.org/10.1101/756700; this version posted September 4, 2019. The copyright holder for this preprint (which was not certified by peer review) is the author/funder. All rights reserved. No reuse allowed without permission.

Keyes GJ, Paolillo DJ, Sorrells ME. 1989. The Effects of Dwarfing Genes Rht1 and Rht2 on Cellular Dimensions and Rate of Leaf Elongation in Wheat. Annals of Botany **64**, 683–690.

Kirby EJM. 1988. Analysis of leaf, stem and ear growth in wheat from terminal spikelet stage to anthesis. Field Crops Research **18**, 127–140.

Kirchgessner N, Liebisch F, Yu K, Pfeifer J, Friedli M, Hund A, Walter A. 2016. The ETH field phenotyping platform FIP: a cable-suspended multi-sensor system. Functional Plant Biology **44**, 154-168.

Kiss T, Dixon LE, Soltész A, *et al.* 2017. Effects of ambient temperature in association with photoperiod on phenology and on the expressions of major plant developmental genes in wheat (Triticum aestivum L.). Plant, Cell & Environment **40**, 1629–1642.

Kollers S, Rodemann B, Ling J, *et al.* 2013. Whole Genome Association Mapping of Fusarium Head Blight Resistance in European Winter Wheat (Triticum aestivum L.). PLOS ONE **8**, e57500.

Kronenberg L, Yu K, Walter A, Hund A. 2017. Monitoring the dynamics of wheat stem elongation: genotypes differ at critical stages. Euphytica **213**, 157.

Lawit SJ, Wych HM, Xu D, Kundu S, Tomes DT. 2010. Maize DELLA Proteins dwarf plant8 and dwarf plant9 as Modulators of Plant Development. Plant and Cell Physiology **51**, 1854–1868.

Liu X, Huang M, Fan B, Buckler ES, Zhang Z. 2016. Iterative Usage of Fixed and Random Effect Models for Powerful and Efficient Genome-Wide Association Studies. PLOS Genetics **12**, e1005767.

Miralles DJ, Slafer GA. 2007. PAPER PRESENTED AT INTERNATIONAL WORKSHOP ON INCREASING WHEAT YIELD POTENTIAL, CIMMYT, OBREGON, MEXICO, 20–24 MARCH 2006 Sink limitations to yield in wheat: how could it be reduced? The Journal of Agricultural Science 145, 139–149.

Nagelmüller S, Kirchgessner N, Yates S, Hiltpold M, Walter A. 2016. Leaf Length Tracker: a novel approach to analyse leaf elongation close to the thermal limit of growth in the field. Journal of Experimental Botany **67**, 1897–1906.

Parent B, Millet EJ, Tardieu F. 2018. The use of thermal time in plant studies has a sound theoretical basis provided that confounding effects are avoided. Journal of Experimental Botany **70**, 2359–2370.

Parent B, Tardieu F. 2012. Temperature responses of developmental processes have not been affected by breeding in different ecological areas for 17 crop species. New Phytologist **194**, 760–774.

Porter JR, Gawith M. 1999. Temperatures and the growth and development of wheat: a review. European Journal of Agronomy **10**, 23–36.

Purcell S, Neale B, Todd-Brown K, *et al.* 2007. PLINK: a tool set for whole-genome association and population-based linkage analyses. American Journal of Human Genetics **81**, 559–575.

bioRxiv preprint doi: https://doi.org/10.1101/756700; this version posted September 4, 2019. The copyright holder for this preprint (which was not certified by peer review) is the author/funder. All rights reserved. No reuse allowed without permission.

R Core Team. 2018. *R: A language and environment for statistical computing*. Vienna, Austria: R Foundation for Statistical Computing.

Rezaei EE, Siebert S, Hüging H, Ewert F. 2018. Climate change effect on wheat phenology depends on cultivar change. Scientific Reports **8**, 4891.

Rodríguez-Álvarez MX, Boer MP, van Eeuwijk FA, Eilers PHC. 2018. Correcting for spatial heterogeneity in plant breeding experiments with P-splines. Spatial Statistics **23**, 52–71.

Roth L, Aasen H, Walter A, Liebisch F. 2018. Extracting leaf area index using viewing geometry effects—A new perspective on high-resolution unmanned aerial system photography. ISPRS Journal of Photogrammetry and Remote Sensing **141**, 161–175.

Sanchez-Bermejo E, Balasubramanian S. 2016. Natural variation involving deletion alleles of FRIGIDA modulate temperature-sensitive flowering responses in Arabidopsis thaliana. Plant, Cell & Environment **39**, 1353–1365.

Schürch C, Kronenberg L, Hund A. 2018. *Wheat developmental stages*. Available at: https://commons.wikimedia.org/wiki/File:Wheat_developmental_stages.tif (accessed 6 July 2018).

Sharma N, Ruelens P, D'hauw M, Maggen T, Dochy N, Torfs S, Kaufmann K, Rohde A, Geuten K. 2017. A Flowering Locus C Homolog Is a Vernalization-Regulated Repressor in Brachypodium and Is Cold Regulated in Wheat. Plant Physiology **173**, 1301–1315.

Slafer GA, Calderini DF, Miralles DJ. 1996. Yield components and compensations in wheat: opportunities for further increasing yield potential. In: Reynolds MP, Rajaram S, McNab A, eds. Increasing Yield Potential in Wheat: Breaking the Barriers : Proceedings of a Workshop Held in Ciudad Obregón, Sonora, Mexico. Mexico: CIMMYT, 101–133.

Slafer GA, Kantolic AG, Appendino ML, Tranquilli G, Miralles DJ, Savin R. 2015. Chapter 12 - Genetic and environmental effects on crop development determining adaptation and yield. In: Calderini VOSF, ed. Crop Physiology (Second Edition). San Diego: Academic Press, 285–319.

Slafer GA, Rawson HM. 1994. Sensitivity of Wheat Phasic Development to Major Environmental Factors: a Re-Examination of Some Assumptions Made by Physiologists and Modellers. Functional Plant Biology **21**, 393–426.

Slafer GA, Rawson HM. 1995*a*. Rates and Cardinal Temperatures for Processes of Development in Wheat: Effects of Temperature and Thermal Amplitude. Functional Plant Biology **22**, 913–926.

Slafer GA, Rawson HM. 1995*b*. Intrinsic earliness and basic development rate assessed for their response to temperature in wheat. Euphytica **83**, 175–183.

Slafer GA, Rawson HM. 1995*c*. Photoperiod × temperature interactions in contrasting wheat genotypes: Time to heading and final leaf number. Field Crops Research **44**, 73–83.

Tang Y, Liu X, Wang J, *et al.* 2016. GAPIT Version 2: An Enhanced Integrated Tool for Genomic Association and Prediction. The Plant Genome **9**.

bioRxiv preprint doi: https://doi.org/10.1101/756700; this version posted September 4, 2019. The copyright holder for this preprint (which was not certified by peer review) is the author/funder. All rights reserved. No reuse allowed without permission.

Thines B, Harmon FG. 2010. Ambient temperature response establishes ELF3 as a required component of the core Arabidopsis circadian clock. Proceedings of the National Academy of Sciences **107**, 3257–3262.

Trevaskis B, Hemming MN, Dennis ES, Peacock WJ. 2007. The molecular basis of vernalization-induced flowering in cereals. Trends in Plant Science **12**, 352–357.

VanRaden PM. 2008. Efficient Methods to Compute Genomic Predictions. Journal of Dairy Science **91**, 4414–4423.

Wang S, Wong D, Forrest K, *et al.* 2014. Characterization of polyploid wheat genomic diversity using a high-density 90 000 single nucleotide polymorphism array. Plant Biotechnology Journal **12**, 787–796.

Whitechurch EM, Slafer GA, Miralles DJ. 2007. Variability in the Duration of Stem Elongation in Wheat and Barley Genotypes. Journal of Agronomy and Crop Science **193**, 138–145.

Wigge PA. 2013. Ambient temperature signalling in plants. Current Opinion in Plant Biology **16**, 661–666.

Wu J, Kong X, Wan J, *et al.* 2011. Dominant and Pleiotropic Effects of a GAI Gene in Wheat Results from a Lack of Interaction between DELLA and GID1. Plant Physiology **157**, 2120–2130.

Xue W, Xing Y, Weng X, *et al.* 2008. Natural variation inGhd7 is an important regulator of heading date and yield potential in rice. Nature Genetics **40**, 761–767.

Yates S, Mikaberidze A, Krattinger S, *et al.* 2018. Precision phenotyping reveals novel loci for quantitative resistance to septoria tritici blotch in European winter wheat. bioRxiv, https://doi.org/10.1101/502260.

Youssefian S, Kirby EJM, Gale MD. 1992. Pleiotropic effects of the GA-insensitive Rht dwarfing genes in wheat. 1. Effects on development of the ear, stem and leaves. Field Crops Research **28**, 179–190.

Zanke CD, Ling J, Plieske J, *et al.* 2014*a*. Genetic architecture of main effect QTL for heading date in European winter wheat. Frontiers in Plant Science **5**, 217.

Zanke C, Ling J, Plieske J, *et al.* 2014*b*. Whole Genome Association Mapping of Plant Height in Winter Wheat (Triticum aestivum L.). PLoS ONE **9**.

Zhang Z, Ersoz E, Lai C-Q, *et al.* 2010. Mixed linear model approach adapted for genome-wide association studies. Nature Genetics **42**, 355–360.

Zheng X, Levine D, Shen J, Gogarten SM, Laurie C, Weir BS. 2012. A high-performance computing toolset for relatedness and principal component analysis of SNP data. Bioinformatics **28**, 3326–3328.

Zikhali M, Griffiths S. 2015. The Effect of Earliness per se (Eps) Genes on Flowering Time in Bread Wheat. Advances in Wheat Genetics: From Genome to Field. Springer, Tokyo, 339–345.

bioRxiv preprint doi: https://doi.org/10.1101/756700; this version posted September 4, 2019. The copyright holder for this preprint (which was not certified by peer review) is the author/funder. All rights reserved. No reuse allowed without permission.

Figures

Fig. 1

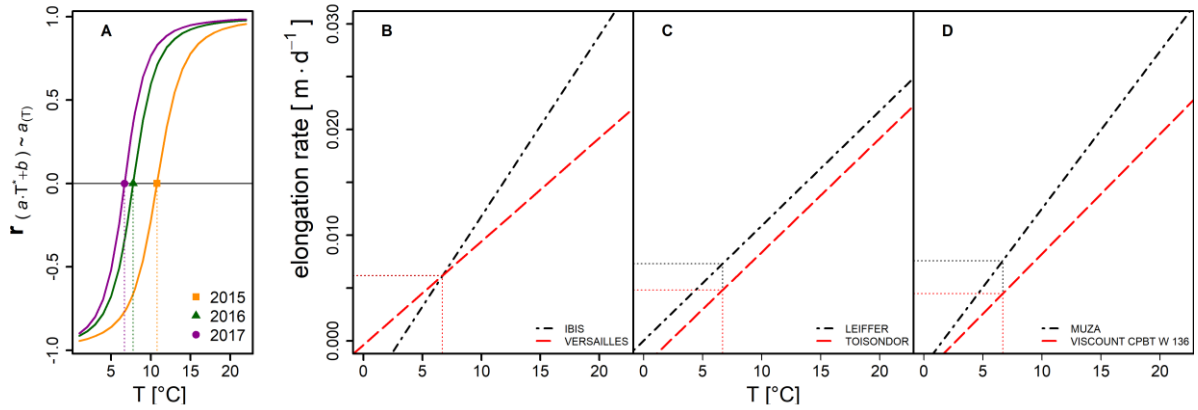

Fig. 1: Illustration and interpretation for the parameters of the applied temperature response model (eq. 2). A: Distribution of Pearson correlation coefficients between intercept and slope of the linear model for individual years, depending on the temperature, at which the intercept is estimated. Dotted vertical lines indicate the critical temperature (T_{crit}) for individual years used to estimate the intercept. **B-D**: Illustration of the relation between intercept and slope on contrasting genotypes (dashed and dash-dotted lines). **B**: same *vigour* but different in temperature-response. **C** both have the same T-response but differ in vigour. **D** Genotypes differ in vigour as well as in T-response. Horizontal and vertical dotted lines indicate vigour and T_{crit} respectively. The two contrasting genotypes per example (**B-D**) were selected from the 2017 data based on their vales for slope and intercept.

bioRxiv preprint doi: https://doi.org/10.1101/756700; this version posted September 4, 2019. The copyright holder for this preprint (which was not certified by peer review) is the author/funder. All rights reserved. No reuse allowed without permission.

Fig.2

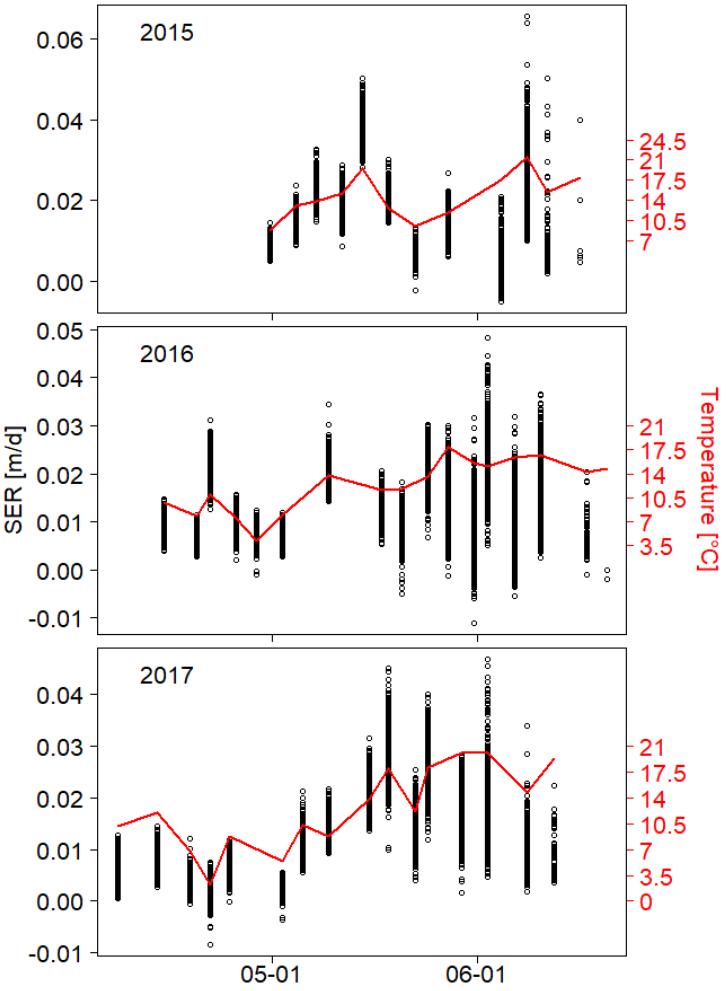

Fig. 2: Relationship between stem elongation rate (SER) and temperature. Plot based SER raw data (n > 700/a) of > 330 genotypes (black dots) as well as temperature (solid red line) is plotted against calendar time for the years 2015-2017.

bioRxiv preprint doi: https://doi.org/10.1101/756700; this version posted September 4, 2019. The copyright holder for this preprint (which was not certified by peer review) is the author/funder. All rights reserved. No reuse allowed without permission.

Fig 3

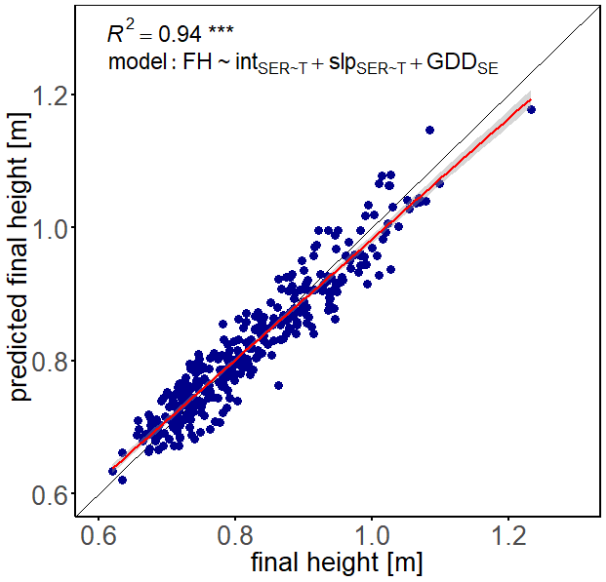

Fig. 3: Prediction of final height using BLUPs for slope and intercept of temperature response and the temperature sum in stem elongation. The linear model $FH \sim int_{SER\sim T} + slp_{SER\sim T} + GDD_{SE}$ was trained on BLUPs across 3 years and tested on the BLUPs of the year 2017.

bioRxiv preprint doi: https://doi.org/10.1101/756700; this version posted September 4, 2019. The copyright holder for this preprint (which was not certified by peer review) is the author/funder. All rights reserved. No reuse allowed without permission.

Fig 4

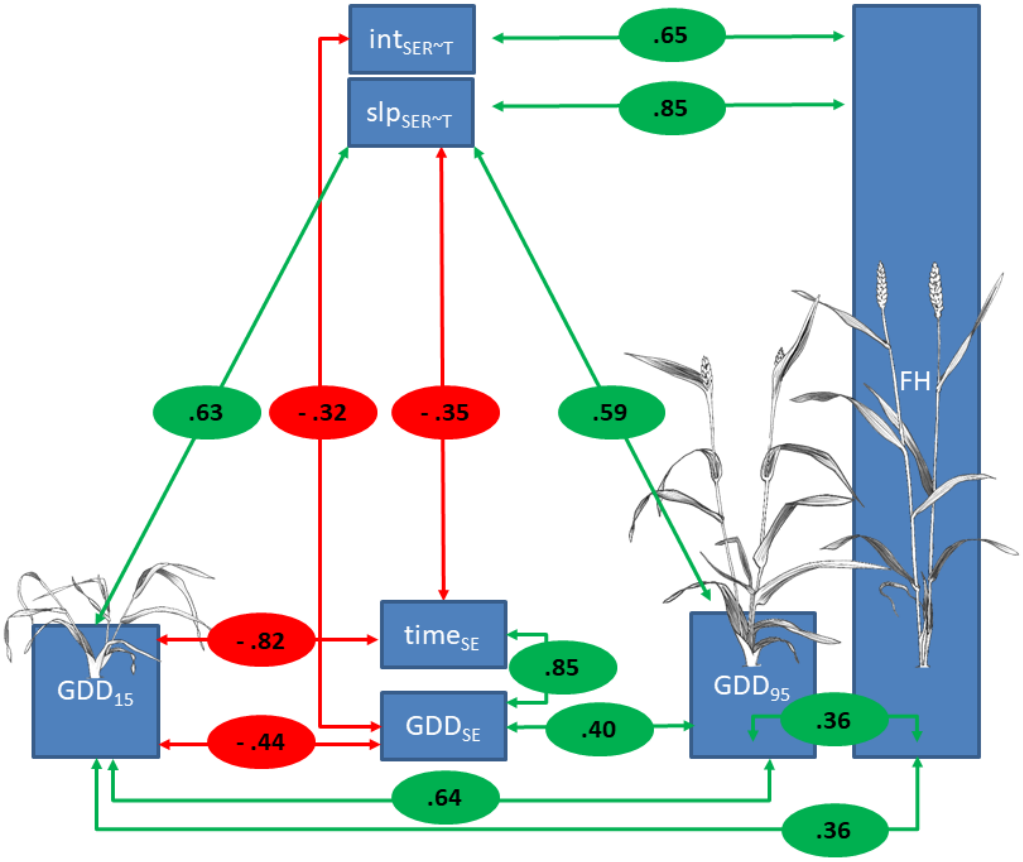

Fig. 4: Key correlations among investigated traits. Pearson correlation coefficients between respective traits are given in red and green circles, where red denotes a negative correlation and green denotes a positive correlation. Weak correlations (r < 0.3) are shown in the complete correlation matrix Fig. S2. Illustrations of GDD_{15}, GDD_{95} and FH were taken from Schürch *et al.* (2018).

bioRxiv preprint doi: https://doi.org/10.1101/756700; this version posted September 4, 2019. The copyright holder for this preprint (which was not certified by peer review) is the author/funder. All rights reserved. No reuse allowed without permission.

Fig 5

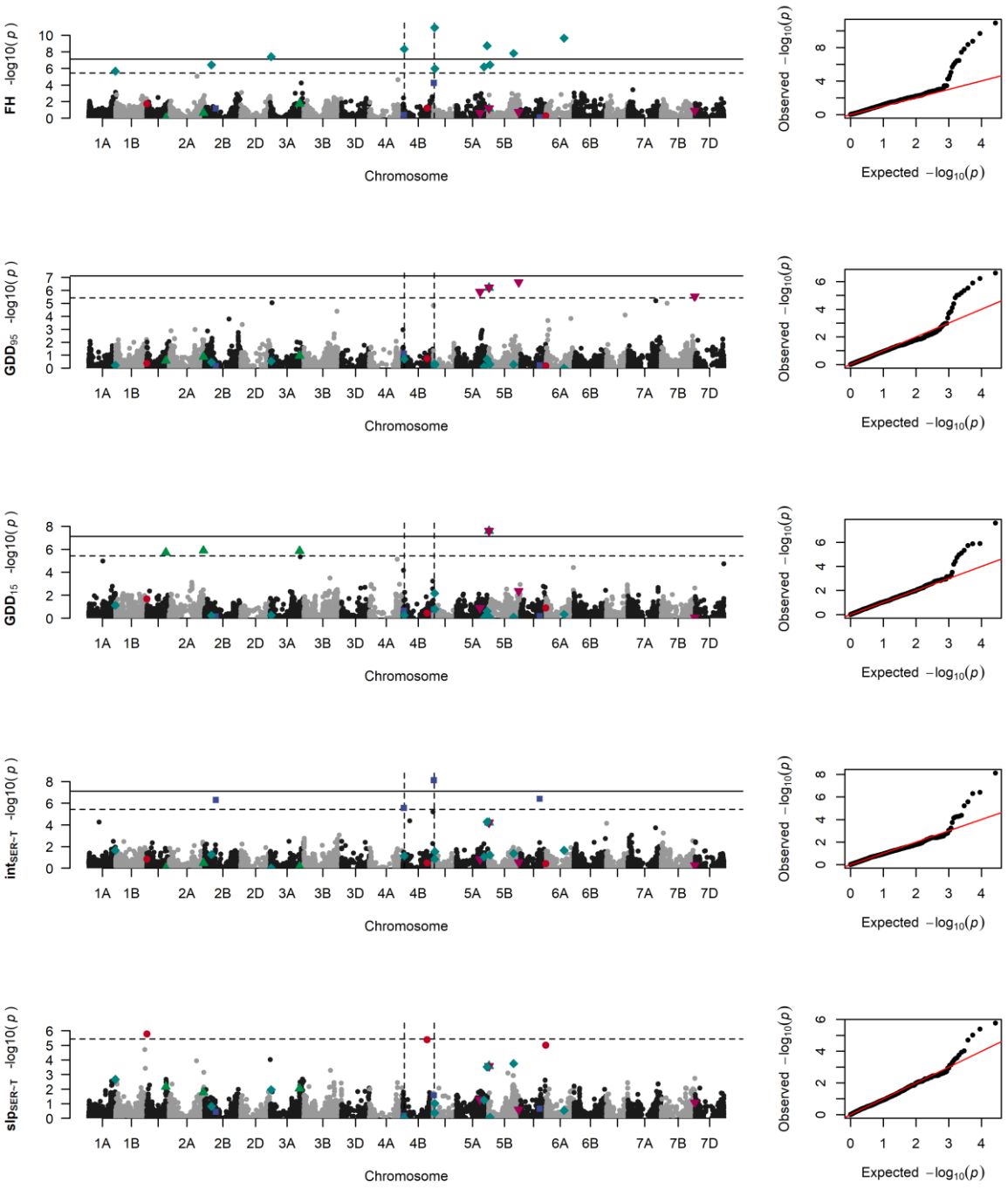

Fig. 5: Manhattan plots and quantile-quantile plots depicting the GWAS results using FarmCPU for final height (FH), growing degree days until start (GDD_{15}) and end (GDD_{95}) of stem elongation; vigour-related intercept ($int_{GR\sim T}$) and temperature-related slope ($slp_{GR\sim T}$) of stem elongation in response to temperature. Horizontal lines mark the Bonferroni corrected significance threshold for $P < 0.05$ (dashed line) and $P < 0.001$ (solid line). Dashed vertical lines mark the position of Rht-B1 and Rht-D1 on chromosome 4B and 4D, respectively. Significant marker trait associations for $slp_{GR\sim T}$ (red dots), $int_{GR\sim T}$ (blue squares), GDD_{15} (green up-facing triangles), GDD_{95} (purple down-facing triangles) and FH (turquois diamonds) are highlighted in all Manhattan plots.

bioRxiv preprint doi: https://doi.org/10.1101/756700; this version posted September 4, 2019. The copyright holder for this preprint (which was not certified by peer review) is the author/funder. All rights reserved. No reuse allowed without permission.

Fig 6

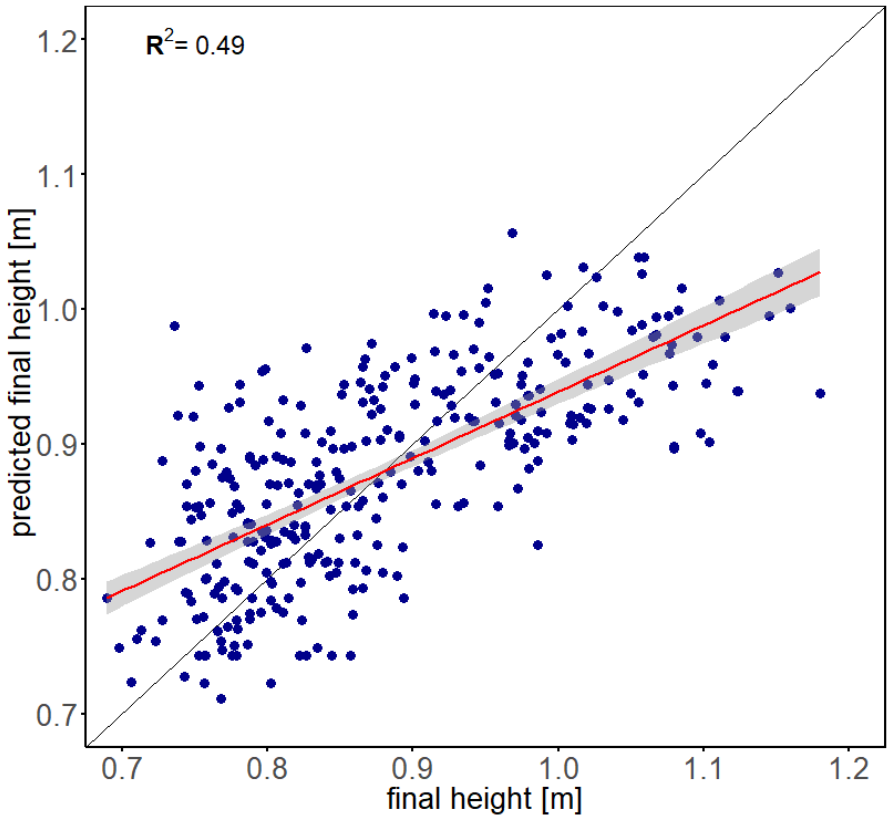

Fig. 6: Prediction of final height using the SNP alleles of significantly associated QTL for temperature response, vigour, start and end of stem elongation as predictors with the linear model:

$FH = QTL\ slp_{SER\sim T} + QTL\ int_{SER\sim T} + QTL\ GDD_{15} + QTL\ GDD_{95}$.

bioRxiv preprint doi: https://doi.org/10.1101/756700; this version posted September 4, 2019. The copyright holder for this preprint (which was not certified by peer review) is the author/funder. All rights reserved. No reuse allowed without permission.

Tables

Table 1

Table 1: Heritabilities of the investigated traits in single years and across all three years.

	heritability			
trait	**BLUPS 2015**	**BLUPS 2016**	**BLUPS 2017**	**3Y-BLUPS**
$int_{GR\sim T}$	0.93	0.95	0.84	0.77
$slp_{GR\sim T}$	0.96	0.91	0.94	0.81
FH	0.99	0.99	0.98	0.98
GDD_{15}	0.93	0.94	0.9	0.82
GDD_{95}	0.75	0.91	0.91	0.84
$time_{SE}$	0.85	0.84	0.85	0.59
GDD_{SE}	0.76	0.83	0.85	0.54

bioRxiv preprint doi: https://doi.org/10.1101/756700; this version posted September 4, 2019. The copyright holder for this preprint (which was not certified by peer review) is the author/funder. All rights reserved. No reuse allowed without permission.

Table 2

Table 2: Marker-trait associations for temperature response, vigour, GDD15, GDD95 and final canopy height, including p-value, allelic effect estimate and minor allele frequency.

Trait	SNP	Chr	Position	p-value	effect	maf
$slp_{GR\sim T}$	wsnp_Ex_c1597_3045682	1B	688'283'256	1.68E-06	-4.90E-05	0.19
	CAP7_c10839_300	4B	533'724'424	4.12E-06	-4.10E-05	0.24
	IAAV7104	5D	553'678'522	9.63E-06	-4.87E-05	0.13
$int_{GR\sim T}$	RAC875_s109189_188	2B	248'149'774	5.10E-07	0.000133	0.42
	Ku_c63300_1309	4B	21'556'672	2.72E-06	-0.00023	0.10
	Kukri_rep_c68594_530	4D	12'773'259	7.45E-09	-0.00018	0.40
	Kukri_c6477_696	5D	423'502'809	3.94E-07	-0.00016	0.21
GDD_{15}	wsnp_Ex_c12447_19847242	1D	416'456'386	1.91E-06	5.680002	0.46
	Tdurum_contig47508_250	2A	754'339'235	1.30E-06	7.757529	0.21
	Kukri_c55381_67	3A	648'868'234	1.38E-06	-8.27442	0.17
	Excalibur_c74858_243	5B	13'190'663	2.50E-08	-6.49833	0.47
GDD_{95}	Excalibur_c49597_579	5A	521'934'666	1.30E-06	-5.483	0.42
	Excalibur_c74858_243	5B	13'190'663	6.08E-07	-5.14378	0.47
	Tdurum_contig44115_561	5B	669'897'388	2.39E-07	-8.48015	0.13
	RAC875_c38693_319	7B	740'056'880	2.92E-06	6.287669	0.20
FH	Excalibur_c85499_232	1A	582'219'427	2.22E-06	0.02035	0.11
	BS00089734_51	2B	150'200'409	3.76E-07	0.018447	0.16
	Kukri_c49280_230	3A	20'134'735	3.88E-08	0.029134	0.08
	Tdurum_contig64772_417	4B	26'491'482	4.58E-09	0.034734	0.07
	RAC875_rep_c105718_585	4D	25'989'162	1.17E-11	-0.02371	0.38
	BS00036421_51	4D	32'347'318	1.06E-06	-0.01463	0.37
	RAC875_c8231_1578	5A	613'588'253	6.47E-07	0.014219	0.43
	wsnp_Ku_rep_c71232_70948744	5A	679'663'586	1.80E-09	-0.02029	0.47
	Excalibur_rep_c72561_141	5B	34'040'001	3.65E-07	-0.03066	0.05
	BS00109560_51	5B	556'182'591	1.49E-08	-0.01766	0.46
	BS00022120_51	6A	396'301'470	2.21E-10	-0.02386	0.24

Table 3

Table 3: Selected putative candidate genes for the intercept of temperature response from the IWGSC reference genome annotation.

Chr	SNP [Position]	r.start	r.end	Gene	description	distance
chr1B	wsnp_Ex_c1597_3045682 [688'283'256]	688'282'509	688'286'431	TraesCS1B01G480600	winged-helix DNA-binding transcription factor family protein	747
		688'352'414	688'354'696	TraesCS1B01G480700	HMG-Y-related protein A	-69'158
		687'710'716	687'719'885	TraesCS1B01G480100	Argonaute	572'540
		687'128'952	687'135'442	TraesCS1B01G479200	Zinc finger protein CONSTANS	1'154'304
		687'078'233	687'084'562	TraesCS1B01G479000	Zinc finger protein CONSTANS	1'205'023
		686'928'468	686'931'886	TraesCS1B01G478700	Zinc finger protein CONSTANS	1'354'788
		686'749'516	686'755'405	TraesCS1B01G478100	WD-repeat protein, putative	1'533'740
		685'645'287	685'649'392	TraesCS1B01G477400	Early flowering 3	2'637'969
chr4B	CAP7_c10839_300 [533'724'424]	537'474'959	537'479'867	TraesCS4B01G266000	Protein FRIGIDA	-3'750'535
		541'363'317	541'365'139	TraesCS4B01G267700	Protein upstream of flc	-7'638'893
		542'582'729	542'583'265	TraesCS4B01G268300	MADS transcription factor	-8'858'305
chr5D	IAAV7104 [553'678'522]	554'357'761	554'360'305	TraesCS5D01G544800	FRIGIDA-like protein, putative	-679'239
		554'467'487	554'472'596	TraesCS5D01G545100	Transducin/WD-like repeat-protein	-788'965
		556'226'523	556'234'480	TraesCS5D01G548800	Transducin/WD-like repeat-protein	-2'548'001

Table 4

Table 4: Selected putative candidate genes for vigour ($int_{SER\sim T}$) of temperature response from the IWGSC reference genome annotation.

Chr	SNP [Position]	r.start	r.end	Gene	description	distance
chr2B	RAC875_s109189_188 [248’149’774]	243'569'388	243'571'100	TraesCS2B01G239400	GRAS transcription factor	4'580'386
chr4B	Ku_c63300_1309 [21’556’672]	21'187'173	21'192'244	TraesCS4B01G028500	Tesmin/TSO1-like CXC domain-containing protein	369'499
		20'005'649	20'008'978	TraesCS4B01G026600	Argonaute family protein	1'551'023
		19'740'974	19'744'058	TraesCS4B01G026200	WD40 repeat-like protein	1'815'698
		23'404'428	23'408'188	TraesCS4B01G031300	BHLH family protein, putative, expressed	-1'847'756
		23'818'506	23'822'972	TraesCS4B01G032000	Protein UPSTREAM OF FLC	-2'261'834
		18'162'363	18'165'744	TraesCS4B01G025500	Homeobox protein BEL1 like	3'394'309
		18'091'908	18'093'975	TraesCS4B01G025400	BEL1-like homeodomain protein	3'464'764
		17'229'197	17'236'874	TraesCS4B01G024000	Argonaute protein	4'327'475
		17'017'132	17'019'148	TraesCS4B01G023300	AGAMOUS-like MADS-box transcription factor	4'539'540
		26'335'682	26'336'740	TraesCS4B01G036600	BRI1 suppressor 1 (BSU1)-like 3	-4'779'010
		26'824'399	26'827'490	TraesCS4B01G037200	WD-repeat protein, putative	-5'267'727
		15'427'017	15'431'870	TraesCS4B01G021500	basic helix-loop-helix (bHLH) DNA-binding superfamily protein	6'129'655
		15'259'656	15'263'139	TraesCS4B01G021200	basic helix-loop-helix (bHLH) DNA-binding superfamily protein	6'297'016
		15'146'117	15'150'854	TraesCS4B01G021100	Basic helix loop helix (BHLH) DNA-binding family protein	6'410'555
		14'710'395	14'711'057	TraesCS4B01G020800	Protein FAR1-RELATED SEQUENCE 5	6'846'277
		28'413'432	28'414'112	TraesCS4B01G041000	sensitive to freezing 6	-6'856'760
		29'673'211	29'674'674	TraesCS4B01G042500	Fantastic four-like protein	-8'116'539
chr4D	Kukri_rep_c68594_530 [12’773’259]	12'700'119	12'703'878	TraesCS4D01G028900	BHLH family protein, putative, expressed	73'140
		13'096'296	13'096'966	TraesCS4D01G029600	CLAVATA3/ESR (CLE)-related protein 25	-323'037
		13'196'859	13'200'535	TraesCS4D01G029700	Protein UPSTREAM OF FLC	-423'600
		11'364'404	11'369'466	TraesCS4D01G026100	Tesmin/TSO1-like CXC domain-containing protein	1'408'855
		10'746'363	10'750'251	TraesCS4D01G024300	Argonaute protein	2'026'896
		10'684'336	10'690'389	TraesCS4D01G024100	Argonaute family protein	2'088'923
		10'254'979	10'257'683	TraesCS4D01G023600	WD40 repeat-like protein	2'518'280
		15'768'990	15'772'059	TraesCS4D01G034500	WD-repeat protein, putative	-2'995'731
		9'495'616	9'501'619	TraesCS4D01G022600	Homeobox protein BEL1 like	3'277'643
		9'443'778	9'445'575	TraesCS4D01G022500	BEL1-like homeodomain protein 1	3'329'481
		9'069'403	9'071'423	TraesCS4D01G021100	MADS-box transcription factor	3'703'856

		16'584'271	16'584'948	TraesCS4D01G038400	sensitive to freezing 6	-3'811'012
		8'777'205	8'779'670	TraesCS4D01G020300	Growth-regulating factor	3'996'054
		8'149'046	8'151'425	TraesCS4D01G019200	basic helix-loop-helix (bHLH) DNA-binding superfamily protein	4'624'213
		8'135'666	8'137'454	TraesCS4D01G019100	basic helix-loop-helix (bHLH) DNA-binding superfamily protein	4'637'593
		8'010'719	8'012'446	TraesCS4D01G018800	basic helix-loop-helix (bHLH) DNA-binding superfamily protein	4'762'540
		7'992'104	7'995'445	TraesCS4D01G018700	basic helix-loop-helix (bHLH) DNA-binding superfamily protein	4'781'155
		17'765'786	17'767'021	TraesCS4D01G039900	Fantastic four-like protein	-4'992'527
		18'781'062	18'782'933	TraesCS4D01G040400	GAI-like protein 1 **(Rht-D1)**	-6'007'803
		6'703'246	6'703'509	TraesCS4D01G015200	SAUR-like auxin-responsive protein family	6'070'013
		6'699'039	6'699'458	TraesCS4D01G015100	SAUR-like auxin-responsive protein family	6'074'220
		6'682'318	6'682'602	TraesCS4D01G015000	SAUR-like auxin-responsive protein family	6'090'941
		6'663'820	6'664'131	TraesCS4D01G014900	SAUR-like auxin-responsive protein family	6'109'439
		6'461'624	6'462'688	TraesCS4D01G013800	BRI1 suppressor 1 (BSU1)-like 3	6'311'635
		19'169'377	19'171'147	TraesCS4D01G040600	Protein FAR1-RELATED SEQUENCE 5	-6'396'118
		6'017'847	6'023'948	TraesCS4D01G012800	Protein FAR1-RELATED SEQUENCE 5	6'755'412
		4'128'933	4'133'919	TraesCS4D01G008400	WD-repeat protein, putative	8'644'326
		21'775'252	21'776'785	TraesCS4D01G046200	CONSTANS-like zinc finger protein	-9'001'993
chr5D	Kukri_c6477_696 [423’502’809]	423'858'756	423'860'766	TraesCS5D01G334100	Armadillo repeat only	-355'947
		421'503'514	421'504'332	TraesCS5D01G329500	HVA22-like protein	1'999'295
		426'296'827	426'301'957	TraesCS5D01G337800	WD-repeat protein, putative	-2'794'018
		429'289'426	429'292'023	TraesCS5D01G341000	CONSTANS-like zinc finger protein	-5'786'617
		416'787'868	416'788'986	TraesCS5D01G325300	Protein Mei2	6'714'941
		416'625'946	416'628'639	TraesCS5D01G325200	Protein Mei2	6'876'863
		415'622'032	415'622'615	TraesCS5D01G323500	Auxin-responsive protein	7'880'777

bioRxiv preprint doi: https://doi.org/10.1101/756700; this version posted September 4, 2019. The copyright holder for this preprint (which was not certified by peer review) is the author/funder. All rights reserved. No reuse allowed without permission.

Table 5

Table 5: Type II analysis of variance of the linear model FH = QTL $slp_{SER\sim T}$ + QTL $int_{SER\sim T}$ + QTL GDD_{15} + QTL GDD_{95}.

QTL	SNP	Sum Sq	Df	F value	Pr(>F)	
$Slp_{SER\sim T}1\_1B$	wsnp_Ex_c1597_3045682	0.021	1	3.364	6.76E-02	
$Slp_{SER\sim T}2\_4B$	CAP7_c10839_300	0.062	1	9.862	1.86E-03	**
$Slp_{SER\sim T}3\_5D$	IAAV7104	0.114	1	18.055	2.87E-05	***
$Int_{SER\sim T}1\_2B$	RAC875_s109189_188	0.018	1	2.828	9.37E-02	
$Int_{SER\sim T}2\_4B$	Ku_c63300_1309	0.122	1	19.318	1.54E-05	***
$Int_{SER\sim T}3\_4D$	Kukri_rep_c68594_530	0.428	1	67.968	5.25E-15	***
$Int_{SER\sim T}4\_5D$	Kukri_c6477_696	0.001	1	0.157	6.92E-01	
$GDD_{15}1\_1D$	wsnp_Ex_c12447_19847242	0.052	1	8.313	4.22E-03	**
$GDD_{15}2\_2A$	Tdurum_contig47508_250	0.075	1	11.970	6.19E-04	***
$GDD_{15}3\_3A$	Kukri_c55381_67	0.002	1	0.298	5.85E-01	
$GDD_{15}4\_5B/GDD_{95}2\_5B$	Excalibur_c74858_243	0.050	1	8.013	4.96E-03	**
$GDD_{95}1\_5A$	Excalibur_c49597_579	0.057	1	9.010	2.91E-03	**
$GDD_{95}3\_5B$	Tdurum_contig44115_561	0.012	1	1.985	1.60E-01	
$GDD_{95}4\_7B$	RAC875_c38693_319	0.002	1	0.326	5.68E-01	
NA	Residuals	1.887	300	NA	NA	